Korean Journal of Remote Sensing, Vol.20, No.5, 2004, pp.289~305

New Methods for Correcting the Atmospheric Effects in Landsat Imagery over Turbid (Case-2) Waters

Yu-Hwan Ahn and P. Shanmugam

Satellite Ocean Research Laboratory

Korea Ocean Research and Development Institute

Abstract : Atmospheric correction of Landsat Visible and Near Infrared imagery (VIS/NIR) over aquatic environment is more demanding than over land because the signal from the water column is small and it carries immense information about biogeochemical variables in the ocean. This paper introduces two methods, a modified dark-pixel substraction technique (path-extraction) and our spectral shape matching method (SSMM), for the correction of the atmospheric effects in the Landsat VIS/NIR imagery in relation to the retrieval of meaningful information about the ocean color, especially from Case-2 waters (Morel and Prieur, 1977) around Korean peninsula. The results of these methods are compared with the classical atmospheric correction approaches based on the 6S radiative transfer model and standard SeaWiFS atmospheric algorithm. The atmospheric correction scheme using 6S radiative transfer code assumes a standard atmosphere with constant aerosol loading and a uniform, Lambertian surface, while the path-extraction assumes that the total radiance (L_{TOA}) of a pixel of the black ocean (referred by Antoine and Morel, 1999) in a given image is considered as the path signal, which remains constant over, at least, the sub scene of Landsat VIS/NIR imagery. The assumption of SSMM is nearly similar, but it extracts the path signal from the L_{TOA} by matching-up the in-situ data of water-leaving radiance, for typical clear and turbid waters, and extrapolate it to be the spatially homogeneous contribution of the scattered signal after complex interaction of light with atmospheric aerosols and Raleigh particles, and direct reflection of light on the sea surface. The overall shape and magnitude of radiance or reflectance spectra of the atmospherically corrected Landsat VIS/NIR imagery by SSMM appears to have good agreement with the in-situ spectra collected for clear and turbid waters, while path-extraction over turbid waters though often reproduces in-situ spectra, but yields significant errors for clear waters due to the invalid assumption of zero water-leaving radiance for the black ocean pixels. Because of the standard atmosphere with constant aerosols and models adopted in 6S radiative transfer code, a large error is possible between the retrieved and in-situ spectra. The efficiency of spectral shape matching has also been explored, using SeaWiFS imagery for turbid waters and compared with that of the standard SeaWiFS atmospheric correction algorithm, which fails in highly turbid waters, due to the assumption that values of water-leaving radiance in the two NIR bands are negligible to enable retrieval of aerosol reflectance in the correction of ocean color imagery. Validation suggests that accurate the retrieval of water-leaving radiance is not feasible with the invalid assumption of the classical algorithms, but is feasible with SSMM.

Key Words : Atmospheric Correction, Spectral Shape Matching Method, Landsat-TM, SeaWiFS, Case-2 water.

Received 12 July 2004; Accepted 16 September 2004.

1. Introduction

Retrieval of ocean color information from remotely sensed imagery is a two-step process: (1) L_w is retrieved as a product of atmospheric correction and (2) the constituents' concentrations are determined from L_w. With the intention of correcting the atmospheric effects in the ocean color imagery, several researchers have developed the atmospheric correction (AC) algorithms, which have increased in complexity from the simple single scattering algorithm designed for the Coastal Zone Color Scanner (CZCS) (Gordon, 1978) to the complex multiple scattering algorithms proposed for SeaWiFS and MERIS (Gordon and Wang, 1994; Antoine and Morel, 1999). The performance of these algorithms were examined and it was found that they perform better in case-1 waters, where the optical properties are determined solely by living algal cells and their associated debris and water itself (Morel and Prieur, 1977), but they are unsuitable for Case-2 waters, which are highly influenced by inorganic mineral particles and additionally by other nonliving dissolved organic materials (DOM). The main reason for the failure of these algorithms over turbid waters is the invalid assumption of zero water-leaving radiance for the near-infrared (NIR) bands at 765 and 865nm, which is common for open ocean waters. Until recently, only few algorithms have been developed (Land and Haigh, 1996; Ruddick *et al.*, 2000; Siegel *et al.*, 2000), which perform reasonably well in the correction of atmospheric effects, resulting from scattering and absorption of Raleigh and aerosol particles in the atmosphere and from direct reflection at the sea surface, from the L_{TOA} measurements by high spectral resolution ocean sensor over Case-2 waters. It is, however, not much emphasis has been given for the correction of atmospheric effects in the high resolution remotely sensed data, from Landsat-TM, SPOT-HRV and IRS-LISS-III sensors, acquired over the ocean because most of the algorithms are more applicable for deriving land cover information (Popp, 1995; Liang *et al.*, 2001). The useful algorithms and methods reported in the literature are as follows: 6S (Second Simulation of the Satellite Signal in the Solar Spectrum) radiative transfer model (Vermote *et al.*, 1997), invariant object (Hall *et al.*, 1991), histogram matching (Richter, 1996), contrast reduction (Tanre *et al.*, 1998) and dark object (Brivio, 2001). With an aim to over come the shortcomings such as assumption of zero water-leaving radiance at NIR bands and limitations in the availability of reasonable techniques, the objectives of the present paper are framed as follows (1) to introduce two atmospheric correction techniques, namely, path-extraction and spectral shape matching method (SSMM), which are implemented and tested on the Landsat and SeaWiFS optical imagery, (2) to compare the efficiency of path-extraction and SSMM with the classical AC algorithms such as the 6S radiative transfer model (Vermote *et al.*, 1997) and the standard SeaWiFS AC algorithm (Gordon and Wang,1994), and (3) to validate the results of path-extraction and SSMM with the help of in-situ data.

2. Atmospheric correction techniques

1) Atmospheric correction with 6S model

The atmospheric correction of the Landsat optical imagery, acquired over the turbid waters of Jin-do and wan-do bays of Korea, has been carried out with the application of 6S radiative transfer model, released by Vermote *et al.* (1997). For each band of the Landsat imagery, the recorded digital values are first converted to radiance at the level of TOA as follows

$$L_{TOA}(\lambda) = \left(\frac{L_{\max}(\lambda) - L_{\min}(\lambda)}{Q_{cal\,\max}} \right) Q_{cal} + L_{\min}(\lambda) \quad (1)$$

where $L_{TOA}(\lambda)$ is the top of atmosphere (TOA) upwelling radiance ($W_m^{-2}\, s_r^{-1}(m^{-1})$ and Q_{cal}, Q_{calmin}, and

Q_{calmax} are the quantized calibrated pixel value in Digital Number (DN), the minimum quantized calibrated pixel value (DN=0) corresponding to $L_{min}(\lambda)$, and the maximum quantized calibrated pixel value (DN=255) corresponding to $L_{max}(\lambda)$, respectively. $L_{min}(\lambda)$ and $L_{max}(\lambda)$ are the spectral radiance that is scaled to Q_{calmin} and Q_{calmax} in $W_m^{-2}\ s_r^{-1}\ \mu_m^{-1}$.

The $L_{TOA}(\lambda)$ was then converted to TOA reflectance, $R_{TOA}(\lambda)$ (unitless) using the following relationship,

$$R_{TOA}(\lambda) = \frac{\pi L_{TOA}(\lambda) d^2}{\mu_s E_s(\lambda)} \quad (2)$$

where $\mu_s = \cos(\theta_s)$, θ_s is the solar zenith angle; $E_s(\lambda)$ ($W_m^{-2}\ \mu_m^{-1}$) is the solar TOA irradiance. The TOA measurements were then corrected for atmospheric effects using the 6S radiative transfer simulation software. $R_{TOA}(\lambda)$ is related to the above water reflectance (R_w, unitless) as given in the following relationship,

$$R_{TOA}(\lambda) = T_g(R_{ar} + R_{ra} + T_d R_w) \quad (3)$$

where R_{ar} and R_{ra} (unitless) are the aerosol and Rayleigh reflectances, respectively; T_g and T_d (unitless) are the gaseous and diffuse transmittances, respectively.

The final atmospherically corrected reflectance (R_{ac}, unitless) is given as,

$$R_{ac} = \frac{R_w}{1 + SR_w} \quad (4)$$

where S (unitless) is the total spherical albedo.

This atmospherically corrected reflectance, divided by π steradians, can be compared to the remote-sensing reflectance: $1/\pi R_{ac}(\lambda) \approx R_{rs}(\lambda)$.

In order to estimate the atmospheric composition over the study area, at the moment of the satellite's overpass, an appropriate atmospheric model defining pressure (mb), temperature (K), water vapour and ozone densities ($g\ m^{-3}$) as functions of altitude (km) was selected. Of the three predefined tropospheric aerosol models (Continental, Maritime, and Urban), a model with maritime aerosols was selected. The aerosol optical thickness (at 550nm) is obtained by integrating the total extinction coefficient, K_{550} (km^{-1})

$$\tau(550) = \int_0^\infty K_{550}(z)dz. \quad (5)$$

The total extinction coefficient is defined as,

$$K_{550}(z) = \sigma_{550} 10^{-3} N(z) \quad (6)$$

where σ_{550} (μm^2) is the extinction cross-section and the aerosol density (N particles cm^{-3}) is a function of visibility (v, km) as shown below,

$$N(z) = \frac{a(z)}{v} b(z) \quad (7)$$

where z is the altitude (km). The relationship was determined by McClatchey *et al.* (1971), with a(z) and b(z) expressed in particles cm^{-2} and part.cm^{-3}, respectively. In-situ remote reflectance measurements were used to validate the atmospheric corrections.

2) Path-extraction

Path-extraction is a conceptually simple and a more efficient method to extract path-radiance from the total radiance recorded at the level of TOA. It is a modified version of the dark-pixel subtraction method, which is known to have a long history and is the most popular method for correcting atmospheric effects in the high spatial resolution VIS/NIR imagery (Kaufman *et al.*, 2000; Brivio *et al.*, 2001; Liang *et al.*, 2001). Significant advantage of this method is that it extracts the L_{path} signal from the image itself without a detailed characterization of the atmosphere and modeling of its effects can be carried out in the atmospheric correction of any low or high-resolution ocean imagery. In fact, it is a first order technique where the lowest radiance value in certain band is subtracted from that band over the entire image. Thus, the principal assumption is that the TOA signal of deep-blue waters, that have the lowest radiance values in the VIS/NIR spectrum, is reduced to the path-radiance because deep-blue waters are often referred to as "black ocean" (Antoine and Morel, 1999). This radiance due to photons scattered by air molecules

and aerosols, and also possibly reflected at the sea surface is assumed to be spatially homogeneous over the spatial range of, at least, one Landsat scene and the diffuse transmittance is taken to be 1 ($L_{TOA} = L_{path} + t_d L_w$; $t_d = 1$, $L_w = 0$). Having done this simple procedure, one can easily retrieve the water-leaving radiance from the pixels of turbid waters, which can be comparable with the in-situ water-leaving radiance spectra. In fact, the atmospheric correction algorithm developed for moderate-resolution imaging spectrometer (MODIS) is based on this principle (Santer *et al.*, 1999).

3) Spectral Shape Matching Method (SSMM)

The idea behind this method is quite simple and easy to implement on any satellite imagery. The principal assumption of this method is that, there are some pixels in any given scene whose spectral form of radiances or reflectances is quite stable and known for typical turbid or clear waters, leading to the extraction of the path signal from L_{TOA} by subtracting the known water-leaving radiance values obtained from the in-situ measurements as given below,

$$L_{path}(\lambda) = L_{TOA}(\lambda) - L_{insitu\text{-}ref}(\lambda) \quad (8)$$

where $L_{insitu\text{-}ref}(\lambda)$ is the typical in-situ reference spectra for clear or turbid waters. The atmospheric path signal ($L_{path}(\lambda)$) is the contribution of the photons, scattered and reflected between the sea surface and satellite sensor. The method of extracting path signal, in this manner, is also referred to as absolute calibration (Chavez, 1996). To retrieve L_w values from the satellite VIS/NIR imagery, with the assumption of constant diffuse transmittance ($t_d = 1$) and homogeneous distribution of aerosols and other particles, the $L_{path}(\lambda)$ is then subtracted from the $L_{TOA}(\lambda)$ measured at the TOA as below,

$$L_w(\lambda) = L_{TOA}(\lambda) - L_{path}(\lambda) \quad (9)$$

One can expect that the shape and magnitude of the retrieved water-leaving radiance spectra should approximately match with the in-situ spectrum over the same region. This atmospheric correction procedure is greatly significant in combination with SSMM, especially over turbid waters where most of the classical atmospheric correction algorithms fail. In contrast to path-extraction, SSMM performs even better for Case-2 waters because L_w is not assumed to be zero ($L_{TOA} = L_{path} + t_d L_w$; $t_d = 1$, $L_w \neq 0$). The efficiency of this method is explored, using Landsat-TM and SeaWiFS imagery (Table 1), and the results are compared with those of other atmospheric correction algorithms. The spectral normalization ($\tilde{L}_{turbid\text{-}TM}$) of the retrieved (SSMM) and in-situ spectra is one of the modes of comparison, which can be expressed as follows,

$$\begin{aligned} &\{L_{TOA}(B1) - L_{path}(B1)\}/\{L_{TOA}(B2) - L_{path}(B2)\} = \\ &\quad \tilde{L}_{turbid\text{-}TM}(B1) \approx L_{insitu\text{-}ref}(B1)/L_{insitu\text{-}ref}(B2) \\ &\quad \vdots \\ &\{L_{TOA}(B4) - L_{path}(B4)\}/\{L_{TOA}(B2) - L_{path}(B2)\} = \\ &\quad \tilde{L}_{turbid\text{-}TM}(B4) \approx L_{insitu\text{-}ref}(B4)/L_{insitu\text{-}ref}(B2) \end{aligned} \quad (10)$$

One of the most significant problems in adopting the path-extraction and SSMM methods is that they may not reproduce water-leaving radiance spectra, when the distribution of aerosol loadings vary dramatically, and thus the assumption of spatial homogeneity aerosol loading of these methods will be violated.

3. Results and discussion

1) Atmospheric correction of Landsat-7 ETM+ Imagery

Based on given geometrical conditions, atmospheric conditions, aerosol model type and aerosol concentration, the atmospheric correction has been performed using 6S radiative transfer code released by Vermote *et al.* (1997), on the VIS/NIR spectral band reflectances of the Landsat-7 ETM+ imagery, acquired over the southwest coastal sea of Korea on 16 April

Table 1. Characteristic features of the Landsat-5 TM VIS/NIR bands and their advantages for monitoring the highly dynamic coastal oceanic features.

Spectral Band	Wavelength (nm)	Spatial Resolution (km)	Description	Characteristics
TM-B1	450~520	0.03	Blue	Pigment absorption
SeaWiFS-B1	402~422	1.1	Blue	
SeaWiFS-B2	433~453	1.1	Blue	
SeaWiFS-B3	480~500	1.1	Cyan	
TM-B2	520~600	0.03	Green	Pigment and particles scattering
SeaWiFS-B4	500~520	1.1	Green	
SeaWiFS-B5	545-565	1.1	Green	
TM-B3	630~690	0.03	Red	Pigment absorption
SeaWiFS-B6	660-680	1.1	Red	
TM-B4	760~900	0.03	Near infrared	Atmospheric correction
SeaWiFS-B7	745~785	1.1	Near infrared	
SeaWiFS-B8	845~885	1.1	Near infrared	

2000. Figs. 1a-d show the TOA reflectance (R_{TOA}) in the center wavebands (nm) of the Landsat-7 ETM+ imagery, 485, 560, 660 and 830, respectively. Radiative transfer simulations were carried out to generate path reflectance (R_{path}) values for four VIS/NIR wavelengths, several geometries (θ_s, θ_v, Δ_φ) and optical thicknesses.

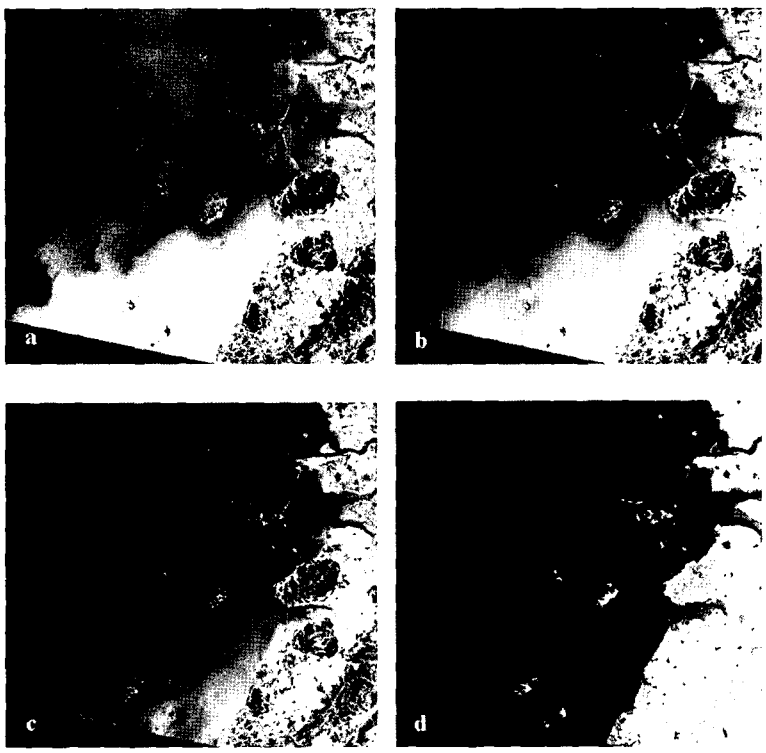

Figs. 1a-d. Maps showing total reflectance at the top of the atmosphere (R_{TOA}) in the center wavebands (nm), 485, 560, 660 and 830, respectively, of the Landsat-7 ETM+ imagery acquired on 16 April 2001, over the southwest coastal waters of Korea.

The same geometries and wavelengths were considered to calculate R_{ra}. The choice of aerosol models (for example, continental aerosol, urban aerosol and maritime aerosol) is critical, particularly regarding their spectral optical thicknesses. Thus, assumptions about the composition and vertical distribution of these aerosols are commonly made, when constructing any classical AC algorithm. Among the three aerosol models adopted in the present study, the maritime aerosol model was considered as an appropriate (candidate) aerosol model for the computation of atmospheric path signal using 6S model. The motivation for the selection of this aerosol model was that, the aerosols confined within the oceanic boundary layer (all molecules above this layer) is predominantly composed of liquid water, sea-salt particles with a residual background of small continental particles, with sizes about less than 0.05μm (Antoine and Morel, 1999). With the assumption of uniformly mixed aerosols within this layer and computation of TOA total radiances for molecular atmosphere using 6S radiative transfer code, the R_{path} signal was assessed to give rise to the extraction of R_w above the sea surface (Fig. 2a). The normalized value of path reflectance Rpath(N) for maritime aerosols is significantly low, when compared to that for urban and continental aerosols. This implies that, high reflectance can be expected from oceanic boundary layer aerosols. Using the 6S code, the path reflectance R_{path} of maritime aerosols and compound atmospheres, assessed from R_{TOA} of the ETM+ VIS/NIR bands, was then compared to that of the path-extraction and SSMM methods. Fig. 2b compares three atmospheric path reflectances of 6S code, path-extraction and SSMM methods. The normalized value of $R_{path(N)}$ (using ETM+ band 4) decreases as a function of increasing wavelength. One should note that 6S model yields high $R_{path(N)}$ values throughout the visible channels, indicating low-level contribution of the atmospheric path signal to the R_w. On the contrary, the $R_{path(N)}$ values assessed using path-extraction and SSMM methods are comparatively low, which in turn yields high reflectance in all visible bands of ETM+. Consequently, the subtraction of path reflectance from R_{TOA} of the ETM+ VIS/NIR bands gives rise to the atmospherically corrected (R_{ac}) water reflectance spectra, which can be compared with the in-situ spectra.

Figs. 3a-d illustrate the total, path and path-corrected reflectance spectra for clear and turbid waters, using 6S radiative transfer model and SSMM. The result of path-extracted was not included in these figures, as it did not

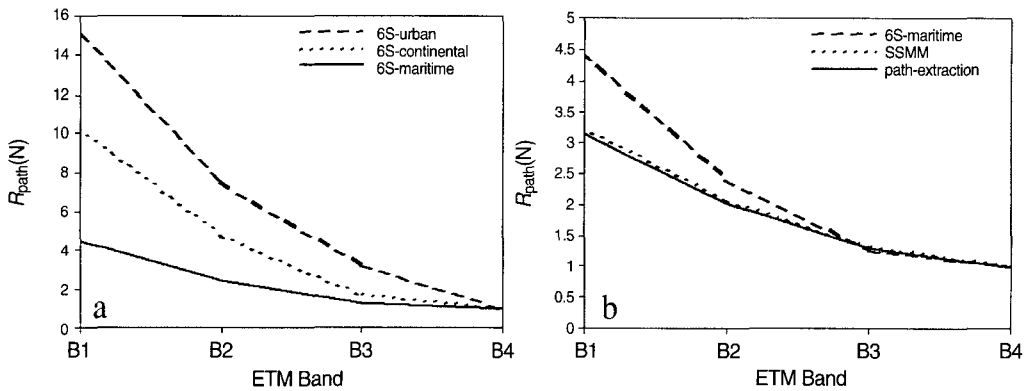

Figs. 2a and b. Comparative performance of three aerosol models (a) and comparison of the path reflectance estimated from the 6S radiative transfer code, developed by Vermote *et al.* (1997), path-extraction and SSMM methods (b). Note that the path reflectance R_{path} is normalized at ETM+ band 4.

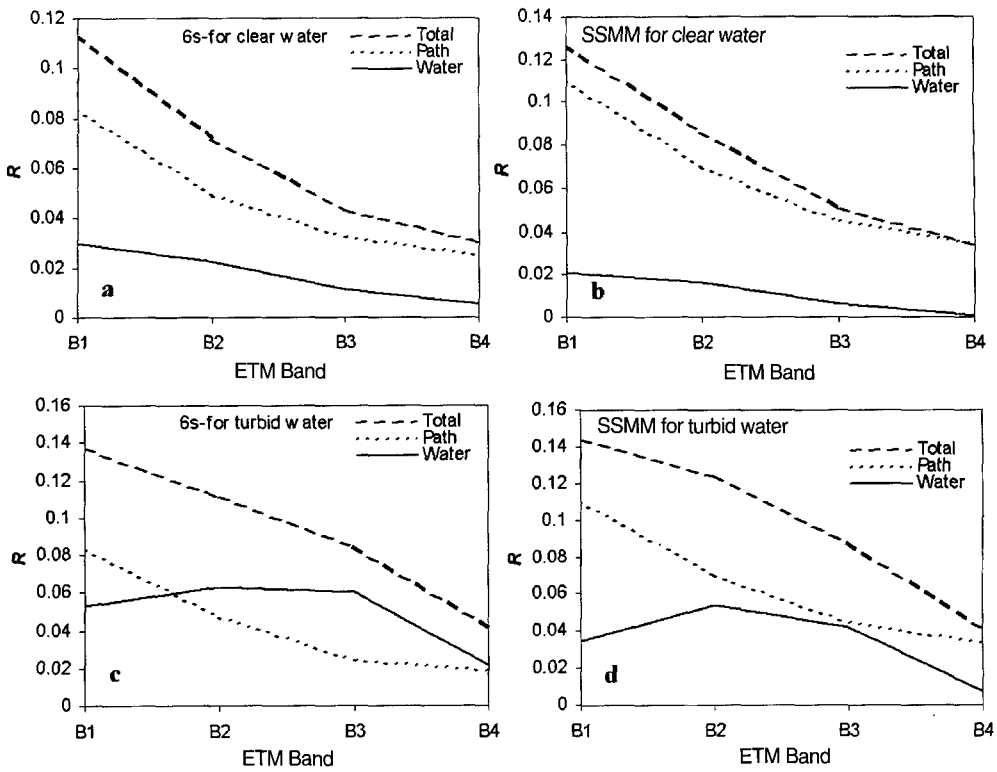

Figs. 3a-d. Schematic representation of the total (at the TOA), path and path-corrected reflectance spectra, obtained from the 6S model and SSMM method, for relatively clear and turbid waters.

have a significant difference from the SSMM method. It is obvious that the total and path reflectances decrease with increasing wavelength. It should be noted that though the spectral form of clear waters is nearly accurate with the 6S model, it often produces unrealistic estimates of R_w values for such waters (Fig.3a). Moreover, it is unable to reproduce the spectral form for turbid waters (Fig. 3c). Conversely, the SSMM method is found to be more efficient in the retrieval of accurate values of R_w and thus the spectral form for both clear and turbid waters (Figs. 3b and d). Appraisal of the results of 6S model, path-extraction and SSMM suggests that, there is a need to compare the derived spectra with the in-situ spectra. To do so, the atmospherically corrected reflectance was divided by π value to obtain the remote-sensing reflectance $R_{rs}(\lambda)$. During the Landsat-7 overpass on 16 April 2001, Simultaneous ground radiometric measurements of surface reflectance (R_{rs}) spectra over clear and turbid water regions were conducted using the ASD (Analytical Spectral Devices) spectroradiometer (covering the spectrum of 0.35-1.1μm). In order to compare the ETM+ band R_{rs} spectra with the in-situ spectra, the ASD measurements were aggregated using the ETM+ sensor spectral response functions for each band. An example is given for ETM+ band2

$$\overline{B}_2(\lambda) = \frac{S(\lambda_1)\times R_{rs}(\lambda_1)+S(\lambda_2)\times R_{rs}(\lambda_2)+S(\lambda_3)\times R_{rs}(\lambda_3)+\cdots+S(\lambda_n)\times R_{rs}(\lambda_n)}{S(\lambda_1)+S(\lambda_2)+S(\lambda_3)+\cdots+S(\lambda_n)} \quad (11)$$

where $S(\lambda)$ is the senstirity for ETM spectral

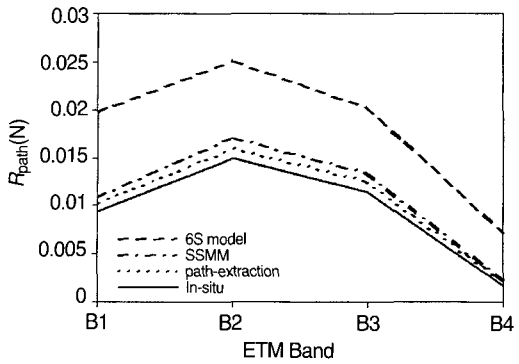

Fig. 4. Comparison of the atmospherically corrected remote sensing reflectance (R_{rs}) spectrum, obtained from 6S model, path-extraction and SSMM, with the in-situ R_{rs} spectrum.

responsivity and $R_{rs}(\lambda)$ is the remote sensing reflectance at 2nm intervals for a given waveband and n is the number of spectral responsivity or R_{rs} for a given ETM waveband. Fig. 4 compares remote sensing reflectance spectra of the ETM+ VIS/NIR bands and in-situ ASD measurements. It is evident that the 6S radiative transfer model leads to the essential overestimation of the R_{rs} values throughout the VIS/NIR spectrum and most importantly, such high values were never observed during our field campaigns in these waters. The main reasons for such unrealistic estimation of R_{rs} values by 6S model are as follows: (1) the selection of generalized atmospheric conditions and a standard aerosol model and concentrations, (2) the introduction of white cape reflectance and (3) the basic assumption itself. Nevertheless the 6S radiative transfer model offers users to define their own real time and ground-observed variables, which can improve the retrieval of water-leaving reflectance in an accurate manner. On the contrary, the SSMM and path-extraction produce spectra, whose form and magnitude are consistent with the in-situ spectra, though slight discrepancies may be associated with these methods, which are attributable to the surface adjacency effects or sub-pixel mixture problems. It is important to note that the close comparison of derived (using path-extraction) and in-situ spectra does not mean that the path-extraction also works well for clear waters, where it yields negatives values of the path-extracted water-leaving radiance or reflectance due to assumption of the black ocean signal.

2) Atmospheric correction of Landsat-5 TM Imagery

The efficiency of SSMM was also explored using the two Landsat-5 TM imageries, acquired on 5 May 1999 and 7 May 2000, over the highly turbid waters of Jin-do and Wan-do bays of Korea. Note that the 2nd image was acquired almost exactly after a period of one-year of obtaining the 1st image. The performance of 6S model could not be assessed, due to lack of ground-observed information. Moreover, it was found in the previous section that the 6S model did not perform well when adopting the standard atmospheric conditions and aerosol models. Figs. 5a and b display the color composite images, generated from the Landsat-5 TM bands (band 4=red, band 3=green, band 2=blue), and show dynamic characteristics of resuspended sediments having similar patterns in both the images. This region is relatively shallow in nature and the depth ranges from 5 to 100m. The suspended sediment concentration (SS) varies from place to place and the maximum suspended sediment concentration observed was between 5~120 g m^{-3}, with the high DOM absorption coefficient varying from 0.1~1.0 m^{-1} at 400nm and chlorophyll concentration ranging from 0.7 to 45mg m^{-3}. A number of field campaigns were conducted for simultaneous radiometric measurements (such as L_u, L_w, Ed^-, Ed^+, L_{sky}) with collection of water samples for the determination of SS, Chl, and DOM concentrations. These regions have been identified as highly turbid in nature for which the L_w or L_u ranges from 0.1 to 1.4 mW cm^{-2} μm^{-1} s_r^{-1} at 555nm, for SS concentration ranging from 1 to 72 g m^{-3} (Figs. 6a and b). It was frequently observed that the range of these values remain constant during SS plume appearance and

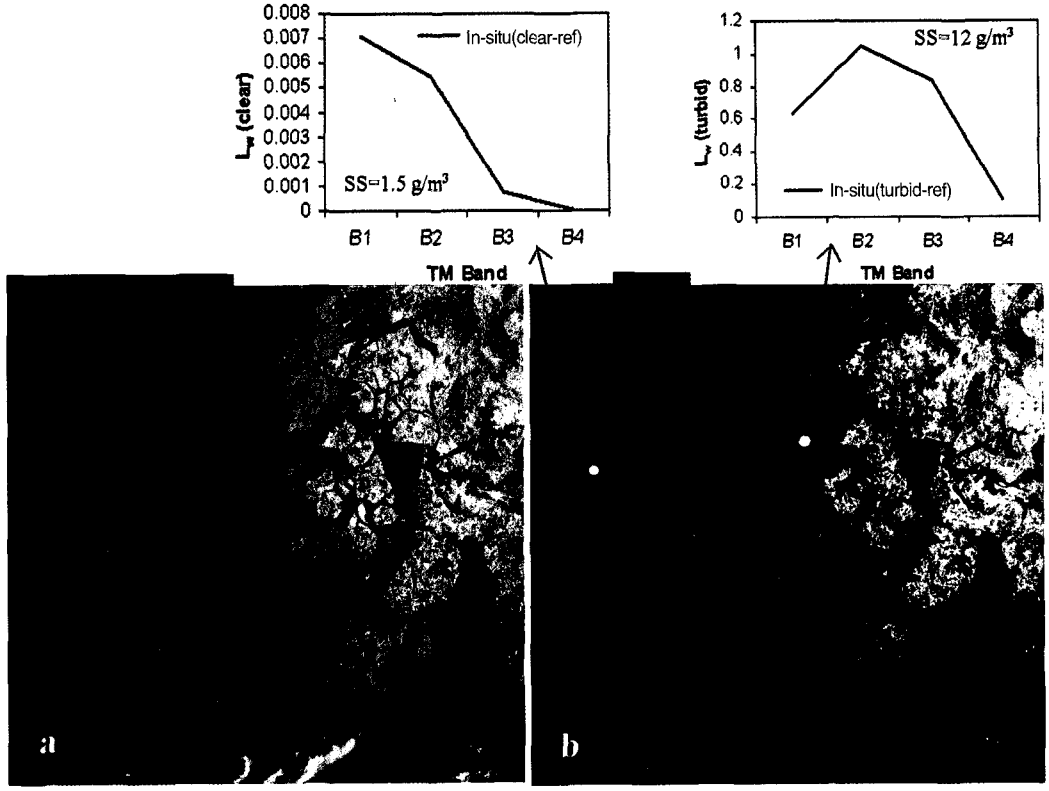

Figs. 5a and b. Color composite images generated from the Landsat-5 TM bands (band 4=red, band 3=green, band 2=blue), acquired on 5 May 1999 (a) and 7 May 2000 (b), showing dynamic characteristics of turbid waters around the southwest coastal areas of Korea. Top panels indicate reference spectra for clear and turbid waters.

propagation in late spring and summer. In order to compare the spectral form of in-situ and TM measurements over typical turbid and clear waters, the in-situ L_u (mW cm^{-2} μm^{-1} sr^{-1}) values just below the

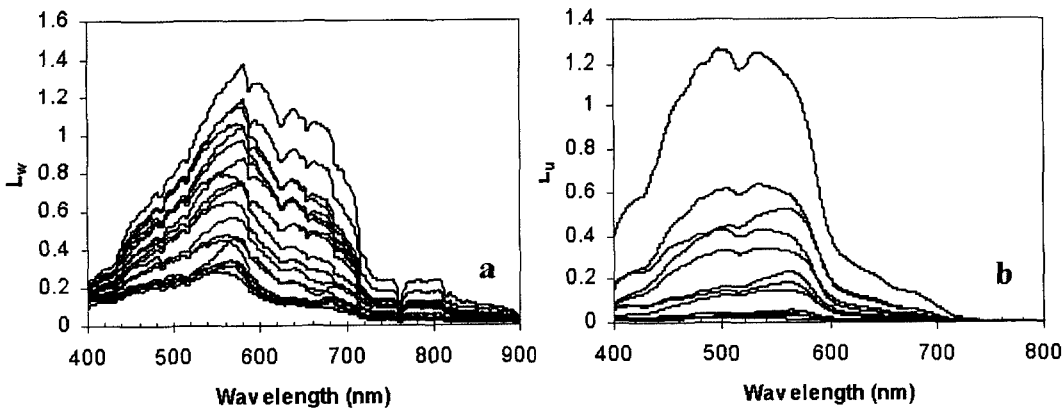

Figs. 6a and b. In-situ water-leaving radiance (L_w) and upwelling radiance (L_u) (m W cm^{-2} μm^{-1} sr^{-1}) spectra observed in the Jin-do and Wan-do turbid waters during Sep.2001and May 2004.

surface, obtained from ASD measurements during May 2004, were first related to L_w just above the surface by considering a constant 0.544, $L_w(\theta, \phi) = 0.544 L_u(\theta, \phi)$, proposed by Austin (1980), and then converted to TM band radiances using normalized response functions of the TM bands (see equation 11). The reference spectra of clear and turbid waters obtained in this way, are illustrated in the top panels of Figs. 5a and b. As the two Landsat imageries were acquired during the same season and month (5 May 1999 and 7 May 2000), with similar characteristics of water masses, it is therefore assumed that, the mean values of L_w of typical turbid or clear water pixels that can be retrieved from the TM bands remains nearly constant under the clear atmospheric conditions. This assumption allows us to extract the path signal from both the imageries using SSMM. Figs. 7a and b illustrates spectra variation of the atmospheric path signal (L_{path}) (mW cm^{-2} μm^{-1} sr^{-1}) over clear (a) and turbid (b) waters, during the overpass of Landsat-5 TM on 5 May 1999 and 7 May 2000. This is to compare variations in the atmospheric path signal between the two imageries over clear and turbid waters. It is observed that the atmospheric path signal (mW cm^{-2} μm^{-1} sr^{-1}) over clear and turbid water regions decreases monotonically, as a function of increasing wavelength for both the Landsat-TM imageries. This implies that absorption by gaseous molecules dominates the longer wavelength part of the electromagnetic (EM) spectrum, while scattering by aerosol particles is more prominent toward the shorter wavelength part of the EM spectrum. A notable difference in the two atmospheric path signals over clear and turbid waters results from the high L_{path} signal of the hazy atmosphere (especially in the southern part of the scene) (please see Fig. 5a) and low L_{path} signal of the clear atmosphere (Fig. 5b).

To assess the importance of the SSMM method, the VIS/NIR imageries of Landsat-5 TM (7 May 2000) were converted to radiance (mW cm^{-2} μm^{-1} sr^{-1}) at the level of TOA (Figs. 8a-d). The brighter pixels indicate high turbidity confined to the coastal waters and darker pixels indicate clear water regions. One should note that the TOA radiance in terms of brightness values constantly decreases with respect to increasing wavelength, but even at low SS concentration it never reaches the zero value at the near infrared spectral domain. Fig. 9a shows spectral variation of the L_{path} signal estimated, using SSMM for the spatially homogeneous atmospheric conditions, over turbid and clear waters. It is apparent that the variation of the L_{path} signal over turbid and clear waters is conspicuously less

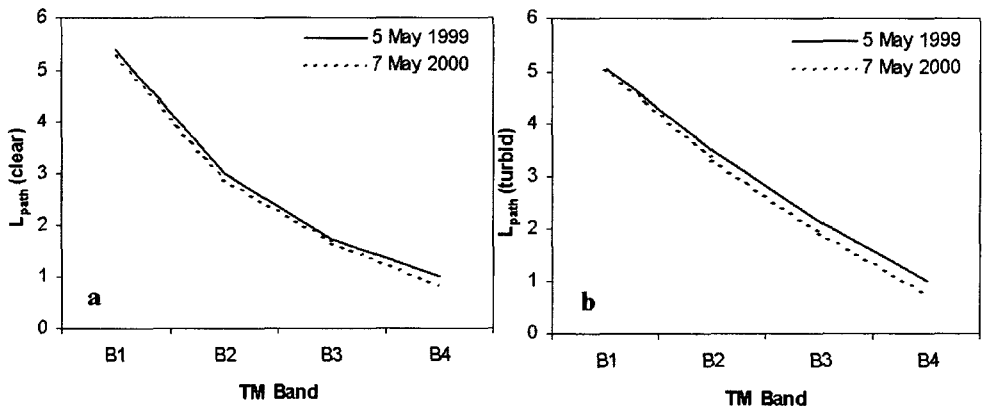

Figs. 7a and b. Spectral variation of the atmospheric path-signal (mW cm^{-2} μm^{-1} sr^{-1}) over clear (a) and turbid waters (b), during the overpass of Landsat-5 TM on 5 May 1999 and 7 May 2000.

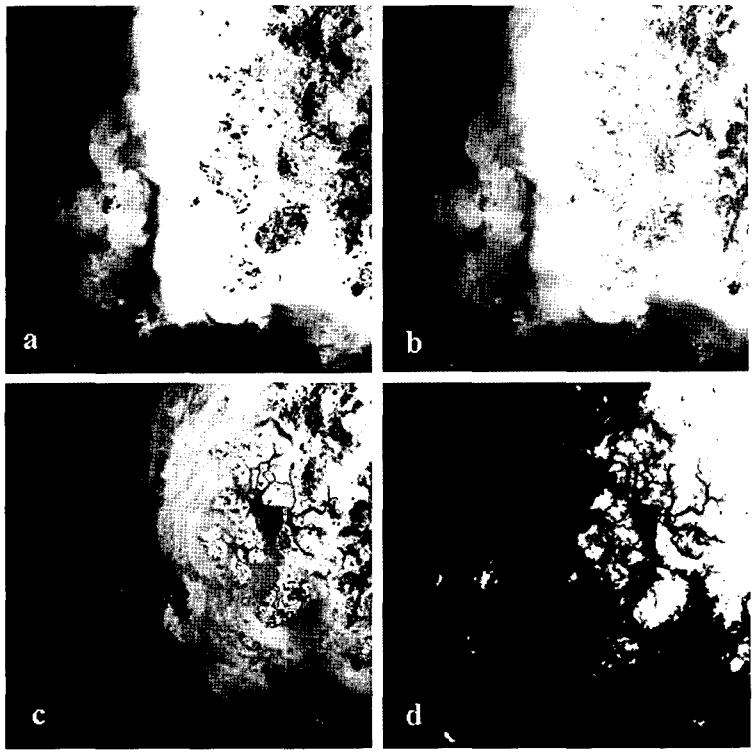

Figs. 8a-d. Maps showing TOA radiances (L_{TOA}) (m W cm^{-2} μm^{-1} sr^{-1}) in the center wavebands (nm), 485 560, 660 and 830, respectively, of the Landsat 5 TM imagery acquired on 7 May 2000 over southwest coastal waters of Korea.

within the coverage of one Landsat scene. Therefore, the mean value of these signals was taken and compared with that of the path-extraction method (Fig. 9b). It should be noted that the high values of L_{path} signal associated with path-extraction might introduce a significant error in the retrieval of water-leaving radiance for clear waters, as a consequence of the assumption of black ocean (i.e. $L_{TOA} = L_{path} + t_d L_w$; t_d =

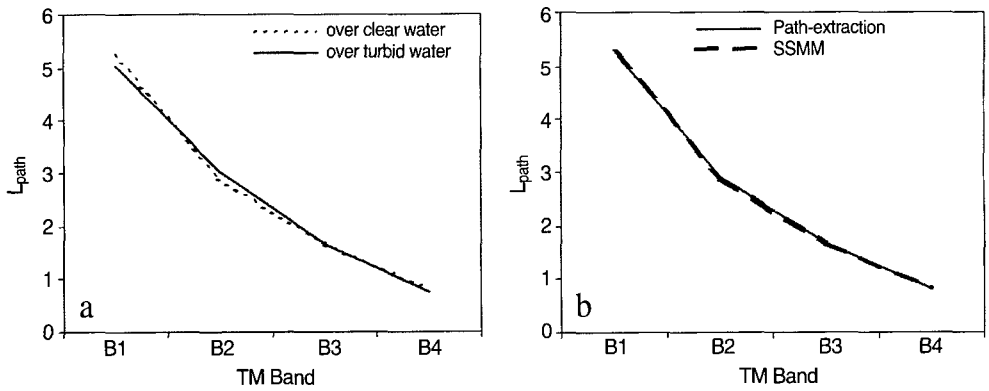

Figs. 9a and b. Spectral variation of the atmospheric L_{path} signal (mW cm^{-2} μm^{-1} sr^{-1}) over clear and turbid water atmospheres, during the Landsat-5 TM overpass on 7 May 2000.

1, L_w = 0). Despite of a lack of number of in-situ observations, validation of the SSMM was performed with the help of in-situ match-up data of upwelling radiance measured during our field campaign in May 2004. Consistent with what is seen with the example from the Jin-do and wan-do bays, there is a very good correlation between in-situ and retrieved L_w spectra from clear waters. As seen in Fig. 10a, under the clear atmospheric conditions deep blue waters scatter light strongly, particularly at the blue wavelength, exhibiting a very steep slope in spectra towards the shorter wavebands of the TM imagery. The steepness lessens for clear waters (Fig. 10b) and a noticeable decline in L_w spectra is evident at this waveband, with a peak at 560nm, when turbidity increases (Fig. 10c). This peak is however no longer stable, and essentially shifts from 560nm towards 660nm, when the level of turbidity remarkably increases due to the occurrence of strong tidal currents and bottom circulations. It is thought that a significant discrepancy between the in-situ and retrieved L_w spectra, particularly for turbid waters, is the result of sub-pixel variability of SS concentration and possibly of the surface adjacency effects, which are caused by the interference of multiply scattered signal from neighboring pixels (Liang, 2001).

3) Extension for correcting the SeaWiFS ocean color imagery

The potential use of SSMM has also been extended to correct the atmospheric effects in the SeaWiFS (Sea-viewing Wide Field-of-View Sensor) ocean color imagery of the same region (turbid waters), acquired on

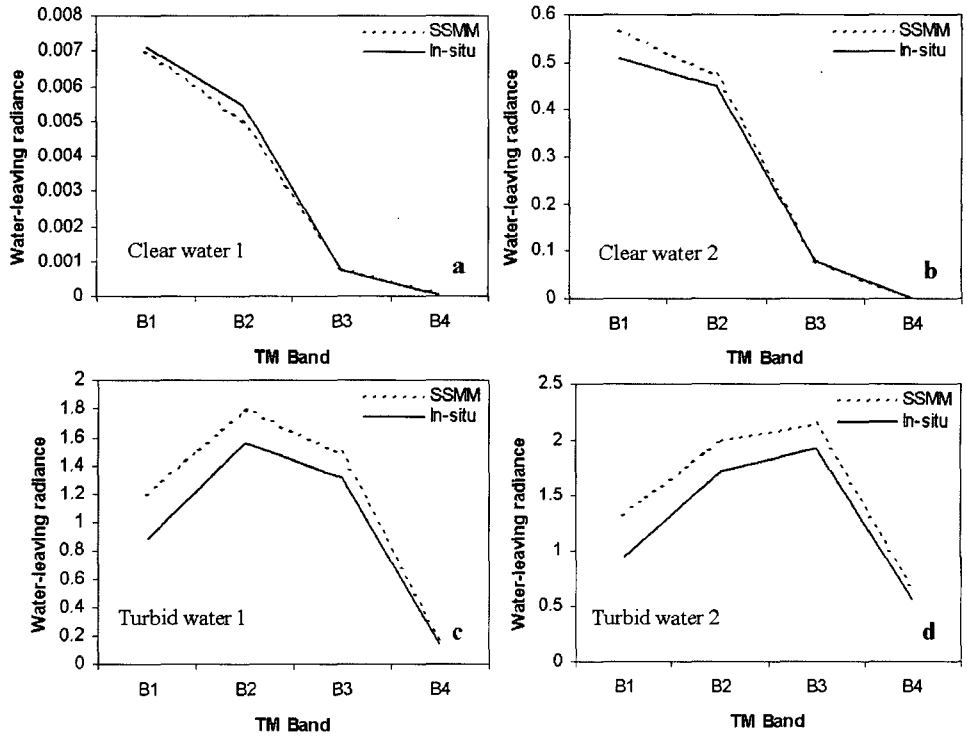

Figs. 10a-d. Comparison of in-situ ASD-radiometric measurements of water-leaving radiance (mW cm^{-2} μm^{-1} sr^{-1}), collected during May 2004, with the spectra retrieved from Landsat-5 TM imagery using the SSMM method (Note that the time of in-situ observation does not coincide with the satellite measurement).

21 October 1998, because the SeaWiFS is exclusively meant for ocean color observations (Hooker *et al.* 1994) and has high spectral resolution bands of 6 visible and 2 NIR, which are severely contaminated by aerosols. It has repeatedly been observed that, the AC algorithm developed for the SeaWiFS sensor, by Gordon and Wang (1994), fails in turbid waters, due to the assumption that values of water-leaving radiance in the two near-infrared (NIR) bands are negligible to enable retrieval of aerosol reflectance in the correction of ocean color imagery (Ruddick *et al.*, 2000). For the purpose of comparison of the SSMM method with the standard SeaWiFS AC algorithm, the water leaving radiance was retrieved from the TOA total signal of Level 1A SeaWiFS product, using the standard atmospheric correction algorithm, which is available in SeaDAS software (Version 4.3). Implementation of the SSMM method necessitates the digital counts of Level 1A raw data to be converted to the total radiance (mW cm^{-2} μm^{-1} sr^{-1}) at the level of the top of the atmosphere. This was done using the SeaWiFS band sensitivity and pre-launch calibration coefficients given in NASA SeaWiFS technical report by Hooker *et al.* (1994). The L_{path} radiance was then retrieved, by taking into account clear and turbid water-leaving radiances. Figs. 11a-d illustrate the assessment of L_{path} radiance over clear and turbid water atmosphere, using the standard SeaWiFS AC algorithm and SSMM. It is interesting to note that, the spectral form and magnitude of L_{path} radiance for clear and turbid water atmospheres, with the standard SeaWiFS AC algorithm, have similar

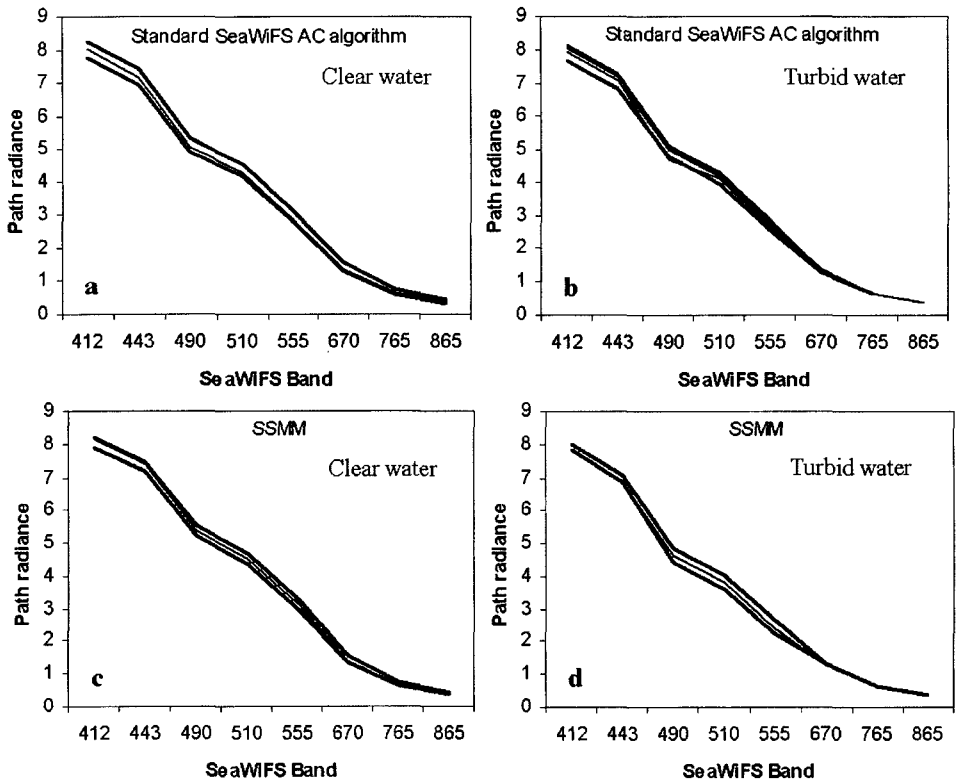

Figs. 11a-d. Variation of the atmospheric path signal (mW cm^{-2} μm^{-1} sr^{-1}) over clear and turbid waters, assessed from total radiance recorded at the TOA by SeaWiFS ocean sensor, flown on 21 October 1998 over the south sea, using the standard SeaWiFS atmospheric correction algorithm and SSMM.

trend with those assessed using the SSMM method. There exists a significant variation in the L_{path} signal of the clear and turbid water atmospheres with the standard SeaWiFS AC algorithm. Having a small variation in the L_{path} signal with SSMM allows a mean value of these signals to be assumed as spatially constant, at least, over the subscene of SeaWiFS image, to retrieve the desired water-leaving radiance. For assessing the efficiency of atmospheric correction using these two methods, the retrieved water-leaving radiances were validated with the in-situ measurements. As done in the previous section, the in-situ ASD measurements of water-leaving radiance were aggregated using SeaWiFS response functions and sensitivity. It is worth noting that, the standard SeaWiFS algorithm leads to the essential overestimation of the L_w values towards the blue-green part of the spectrum, with large errors for highly turbid coastal waters at stations B2 and B3 (Figs. 12 a and b). The concentrations of chlorophyll (Chl), suspended sediments (SS) and dissolved organic matter (DOM) at stations B2 and B3 observed are as follows: St. B2: <Chl> 1.1 mg m^{-3}; <SS> 24 g m^{-3}; <DOM> 0.11 m^{-1}. St. B3: <Chl> 0.7 mg m^{-3}; <SS> 20 g m^{-3}; <DOM> 0.21 m^{-1}. In contrast, the retrieval of L_w using the SSMM method remains very well consistent with in-situ spectra, collected simultaneously from stations B2 and B3 during the SeaWiFS overpass on 21 October 1998. A noticeable disparity between the retrieved (using SSMM) and in-situ L_w can explain the principal effect of sub-pixel variability in the low spatial resolution SeaWiFS data.

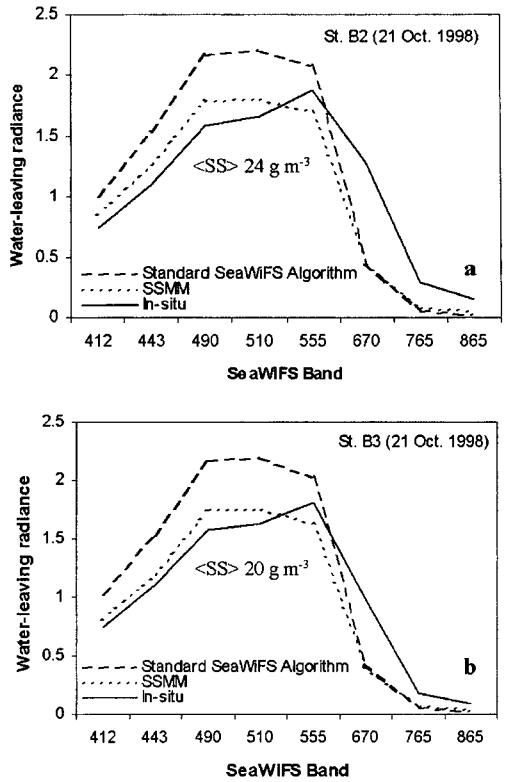

Figs. 12a and b. Comparison of in-situ water-leaving radiance spectra (mW cm^{-2} μm^{-1} sr^{-1}), obtained from ASD measurements in highly turbid waters of the Jin-do and Wan-do bays on 21 October 1998 at 11.45 a.m, with coincident spectra from the SeaWiFS image acquired at 11.31 a.m. and processed with the standard SeaWiFS AC algorithm and SSMM method. The concentrations of chlorophyll (Chl), suspended sediments (SS) and dissolved organic matter (DOM) at stations B2 and B3 are as follows: St. B2: <Chl> 1.1 mg m^{-3}; <SS> 24 g m^{-3}; <DOM> 0.11 m^{-1}. St. B3: <Chl> 0.7 mg m^{-3}; <SS> 20 g m^{-3}; <DOM> 0.21 m^{-1}.

4. Conclusion

The processing of the TOA signal to retrieve ocean reflectance in the VIS/NIR part of the spectrum is always inaccurate in Case-2 waters with the application of classical atmospheric correction algorithms. Two new and efficient methods, to perform atmospheric correction of high spatial resolution Landsat VIS/NIR imagery and high spectral resolution SeaWiFS ocean color imagery for turbid waters, have been described and tested. Due to inadequate ground information and standard atmospheric models or invalid assumption of zero water-leaving radiance at the two NIR bands, by the classical atmospheric correction algorithms, such as the 6S model and standard SeaWiFS AC algorithm,

which misled the desired water-leaving radiance to be essentially overestimated in the visible bands, as the consequence of underestimation of the path radiance or reflectance by these algorithms. Thus, the retrieved water-leaving radiance or reflectance spectra by these algorithms are not comparable with the in-situ spectra. Apart from the basic and invalid assumptions of these algorithms that are responsible for the unrealistic estimation of L_w values, very high signal from turbid waters undergo interference by adjacency signals and complex multiple interactions with the aerosol particles in the atmospheric system, resulting in the introduction of significant errors in the atmospheric correction of the ocean color imagery over turbid waters. Perhaps the classical AC algorithms developed for Case-1 waters need to be treated separately by taking into account the optical properties of turbid waters. In contrast, the path extraction relying on the image itself performs reasonably well for turbid waters, but yields significant errors for clear waters due to invalid assumption of black ocean radiance (as the consequences of typical excessive aerosol path radiance removal). On the other hand, the SSMM seems to be a practical approach because it does not require a detailed characterization of the atmosphere and modeling of multi-component aerosols for the extraction of ocean properties, but relies on match-up in-situ data and the image itself. A preliminary validation of the SSMM made by the comparison of TM or SeaWiFS-derived water-leaving radiance spectra with in-situ measurements for highly turbid waters of the Jin-do and Wan-do bays suggests that, a good reproduction of the water-leaving radiance spectra by this method is possible, with less errors for both clear and turbid waters. Unlike other AC algorithms or methods, the SSMM does consider typical clear and turbid water spectra to derive a constant value of the path signal, which is to be extrapolated over the entire sub-scene of interest towards the retrieval of desired water-leaving radiance. From this study, we feel that these two techniques described in the context of the correcting atmospheric effects in the Landsat VIS/NIR and SeaWiFS imagery are also applicable to other satellite-based (for example, MERIS, MODIS, POLDER, AVHRR etc.) and probably also, airborne ocean color sensors because they do not require number of bands used in the atmospheric correction and modeling of water-leaving radiance at the two NIR wavebands and modeling of DOM absorption at the near ultraviolet band. In the context of chlorophyll retrieval in turbid waters, an atmospheric correction, based on SSMM, is highly complementary to an ocean color model based on red bands and exploiting the chlorophyll absorption peak near 670nm, the chlorophyll fluorescence at 685, or ratio of both (Gower and Borstad, 1990; Ahn *et al.*, 2004). The validation took place only over turbid water regions of Jin-do and Wan-do bays of Korea. Our future work will involve in resolving the horizontal inhomogeneity problem associated with the SSMM technique.

Acknowledgements

The authors would like to acknowledge Ministry of Science and Technology (MOST) and Ministry of Maritime Affairs and Fisheries (MOMAF) for having supported this research work under the KORDI contract No. PM 294-00 and PN 524-00.

References

Ahn Y. H. and P. Shanmugam, 2004. Analysis of sun-induced chlorophyll fluorescence in relation to remote estimation of chlorophyll a concentration in ocean waters, Submitted to the Journal of Plankton Research.

Antoine, D. and A. Morel, 1999. A multiple scattering

algorithm for atmospheric correction of remotely sensed ocean color (MERIS instrument): principle and implementation for atmospheres carrying various aerosols including absorbing ones, *International Journal of Remote Sensing*, 20: 1875-1916.

Austin, R. W., 1980. Gulf of Mexico, ocean-color surface-truth measurements, *Boundary Layer Meteorology*, 18: 269-285.

Brivio, P. A., C. Giardiano, and E. Zilioli, 2001. Determination of concentration changes in Lake Garda using image-based radiative transfer code for Landsat TM images, *International Journal of Remote Sensing*, 22: 487-502.

Chavez, P., 1996. Image-based atmospheric corrections-Revisted and improved, *Photgrammetry Engineering and Remote Sensing*, 62: 1025-1036.

Gordon, H. R., 1978. Removal of atmospheric effects from satellite imagery of the oceans, *Applied Optics*, 17: 1631-1636.

Gordon, H. R. and M. Wang, 1994. Retrieval of water-leaving radiance and aerosol optical thickness over the oceans with SeaWiFS: a preliminary algorithm, *Applied Optics*, 33: 443-452.

Gower, J. F. R. and G.. A. Borstad, 1990. Mapping of phytoplankton by solar solar-stimulated fluorescence using an imaging spectrometer, *International Journal of Remote Sensing*, 11: 313-320.

Hall, F. G., D .E. Strebel., J. E. Nickeson, and S. J. Goetz, 1991. Radiometric rectification: Toward a common radiometric response among multidate, multisensor images, *Remote Sensing of Environment*, 35: 11-27.

Hooker, S. B., E. R. Firestone, and J. G. Acker, 1994. SeaWiFS Pre-launch Radiometric Calibration and Spectral Characterization. *SeaWiFS technical report series, NASA Technical Memorandum* 104566, Vol. 23.

Kaufman, Y. J., A. Karnieli, and D. Tanre, 2000. Detection of dust over deserts using satellite data in the solar wavelengths, *IEEE Transactions of Geoscience and Remote Sensing*, 38: 525-531.

Land, P. E. and J. D. Haigh, 1996. Atmospheric correction over Case-2 waters with an iterative fitting algorithm, *Applied Optics*, 35: 5443-5451.

Liang, S., H. Fang, and M. Chen, 2001. Atmospheric correction of Landsat ETM+ land surface imagery-Part 1: Methods, *IEEE Transaction on Geoscience and Remote Sensing*, 39: 2490-2498.

McClatchey, R. A., R. W. Fenn., J. E. Selby., F. E. Volz, and J. S. Garing, 1971. Optical properties of the atmosphere (revised), AFCRL 71-0279, *Environmental Research Paper* 354, Bedforf, MA, USA.

Morel, A. and L. Prieur, 1977. Analysis of variations in ocean color, *Limnology and Oceanography*, 22: 709-722.

Popp, T., 1995. Correcting atmosphere masking to retrieve the spectral albedo of land surface from satellite measurements, *International Journal of Remote Sensing*, 16: 3483-3508.

Richter R., 1996. A spatially adaptive fast atmospheric correction algorithm, *International Journal of Remote Sensing*, 17: 1201-1214.

Ruddick, K. G., F. Ovidio, and M. Rijkeboer, 2000. Atmospheric correction of SeaWiFS imagery for turbid and inland waters, *Applied Optics*, 39: 897-913.

Santer, R., V. Carrere., P. Dubuisson, and J.C. Roger, 1999. Atmospheric correction over land for MERIS, *International Journal of Remote Sensing*, 20: 1819-1840.

Siegel, D. A., M. Wang., S. Moritorena, and W.

Robinson, 2000. Atmospheric correction of satellite ocean color imagery: the black pixel assumption, *Applied Optics*, 39: 3582-3591.

Tanre, D., P. Y. Deschamps., C. Devaux, and M. Herman, 1998. Estimation of Saharan aerosol optical thickness from blurring effects in Thematic Mapper data, *Journal of Geophysical Research*, 93: 15955-15964.

Vermote, E. F., D. Tanre., J. L. Deuze., M. Herman, and J. J. Morcrette, 1997. Second simulation of the satellite signal in the solar spectrum, AN overview, *IEEE Transactions on Geoscoence and Remote Sensing*, 35: 675-686.